HARMONIC MODAL ANALYSIS USING HYDROELECTRIC RUNNER STEADY-STATE STRAIN GAUGE MEASUREMENTS

Nicolas Morin, Quentin Dollon, Jérôme Antoni, Souheil-Antoine Tahan, Christine Monette, Martin Gagnon

Harmonic Modal Analysis Using Hydroelectric Runner Steady-State Strain Gauge Measurements

Nicolas MORIN[1], Quentin DOLLON[2], Jérôme ANTONI[3], Antoine TAHAN[1], Christine MONETTE[4], Martin GAGNON[2]

[1]Mechanical Engineering Department, ÉTS, Montreal, Montreal, QC, Canada
nicolas.morin.4@ens.etsmtl.ca
[2]Institut de Recherche d'Hydro-Québec (IREQ), Varennes, Canada
[3]Lab. Vibration Acoustique, Univ. Lyon, INSA-Lyon, Villeurbanne, France
[4]Andritz Hydro Canada Inc., Pointe-Claire, QC, Canada

Abstract

The characterization of hydraulic turbine runners' dynamic behaviour is essential for accurate stress and fatigue life prediction leading to design and maintenance adapted to the fluctuating power demand. As the modal parameters of runners depend on the operating regime and coupling effects, a representative estimation of these parameters relies on the analysis of in-operation data. However, harmonics contained in Francis runners strain response complexify the use of traditional operational modal analysis methods. This paper proposes a steady-state harmonic modal analysis method using Non-Trivial Rotor-Casing Interactions (NTRCI). The Bayesian method used to identify the parameters is first presented. The method is evaluated on a ground truth system obtained with an analytically generated strain response and then deployed on operating runner strain gauge measurements. The paper concludes with a discussion and future works related to the exhaustivity of the proposed model.

1 Introduction

Hydroelectric turbines are mechanical systems converting water flow energy to electricity. In a Francis turbine, the spiral casing creates a free water swirl (see Figure 1). The runner transfers water swirl kinetic and potential energy in shaft torque by the transfer of momentum from the deflection of the water. By its function, the runner is one of the most stressed components of the turbine. Runner failure represents a costly loss of production [1]. The recent arrival of intermittent energy sources on the power grid stretches the operating range of hydroelectric turbine-generator units. Off-peak operations of turbines result in new loadings accentuating fatigue degradation of the runner [2,3]. This new reality combined with the financial criticality of the integrity of the runner entails the need to comprehend its dynamic behaviour and loadings. This understanding should improve fatigue analysis, life estimation and diagnosis tools, and allow better-suited design of turbines to the fluctuating demand.

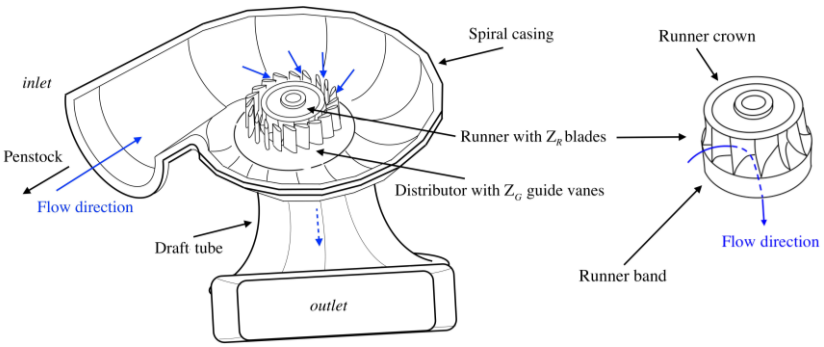

Figure 1: Principal components of Francis turbines
from Dollon et al. (2023)

A typical modal characterization method for the runner is a numerical simulation using an axisymmetric runner in a constrained acoustic fluid volume. The method usually considers isolated components like the runner with or without the shaft. Experimental methods are sometimes used to validate and calibrate numerical simulations [5–7]. Those experimental methods, however, consider the sole runner in air or standstill water ([5,8–10]) which is insufficient to capture the actual fluid-structure coupling effects found in operation. In essence, Operational Modal Analysis (OMA) methods with *in situ* measurements consider the actual geometry of the runner, and coupling and added mass effects. OMA is an output-only identification approach assuming white noise excitation from the environment [11]. Dollon et al. (2020) proposed a Bayesian modal analysis method using strain gauge measurements on runner blades in transient regimes [12]. In steady-state regimes near the Best Efficiency Point (BEP), periodic excitations dominate stochastic excitations, limiting the use of traditional OMA methods. In runner strain measurements, Dollon et al. (2023) observed unexpected resonance between rotation speed harmonics and natural modes of the runner [4]. The author proposed a steady-state periodic forced response model to describe those Non-Trivial Runner-Casing interactions (NTRCI). The proposed model generalizes Rotor-Stator Interactions (RSI) theory [12,13]. The identification of the periodic forced response model using strain gauge measurements presents an opportunity to achieve a harmonic-based modal analysis of the turbine runner.

This paper presents a Bayesian inference method for the harmonic modal analysis of a Francis turbine runner using *in situ* strain gauge measurements. The paper is structured as follows. Section 2 presents the runner blade periodic forced response model. Section 3 proposes an inference methodology to evaluate the runner's NTRCI excitation and modal parameters. Section 4 circumscribes the range of applicability of the algorithm through a synthetic data study. Section 5 presents the implementation of the method on an operational prototype runner under a NTRCI excitation. Section 6 discusses perspectives on future developments and applications of the method before concluding in section 7.

2 Periodic Forced Response Model

Dollon et al. (2023) proposed a model to estimate the forced response of a runner blade to a periodic excitation. The model states that in the modal basis, the excitation generates Q harmonics per nodal diameter v, Q being a number depending on the considered bandwidth. The number of nodal diameters v is a quantity used to characterize the spatial shape of a mode in an axisymmetric structure [9,13]. Runner nodal diameters v are integers from $]-Z_R/2\,,Z_R/2[$ if the number of blades Z_R is odd or $[-Z_R/2\,,Z_R/2]$ if Z_R is even. In this paper, negative nodal diameters are corotating (forward) modes and positive nodal diameters v counterrotating (backward) modes. Nodal diameter $v = 0$ is a standing vibration, considered as a forward mode in the model.

On an observed point n on the blade, the angular position θ dependant shape $F(\theta)$ of the periodic excitation force can be expressed by a set of Fourier coefficients $\{F_p\}$. For a Z_R-bladed runner, the force projected in the modal basis generates an excitation harmonic as expressed in Eq. 1.

$$\boldsymbol{c}_{q,v} = \sum_{p\in\mathbb{Z}} F_p^* \, sinc\left[(q-p)\pi + \frac{\pi v}{Z_R}\right] e^{i\left[(q-p)\pi+\frac{\pi v}{Z_R}\right]} \approx \boldsymbol{F}^{1Z}\boldsymbol{\Phi}_{q,v}^{1Z}\,,\ q \in [1,Q] \tag{1}$$

In Eq. 1, $\boldsymbol{c}_{q,v} \in \mathbb{C}^{N\times 1}$ contains the excitation Fourier coefficients, $\boldsymbol{F}^{1Z} \in \mathbb{C}^{N\times(2P+1)}$ contains a finite quantity P of force Fourier coefficients for a one-per-revolution force, $\boldsymbol{\Phi}_{q,v}^{1Z} \in \mathbb{C}^{(2P+1)\times 1}$ is the transformation vector expressing the excitation force in the modal basis as illustrated in Figure 2

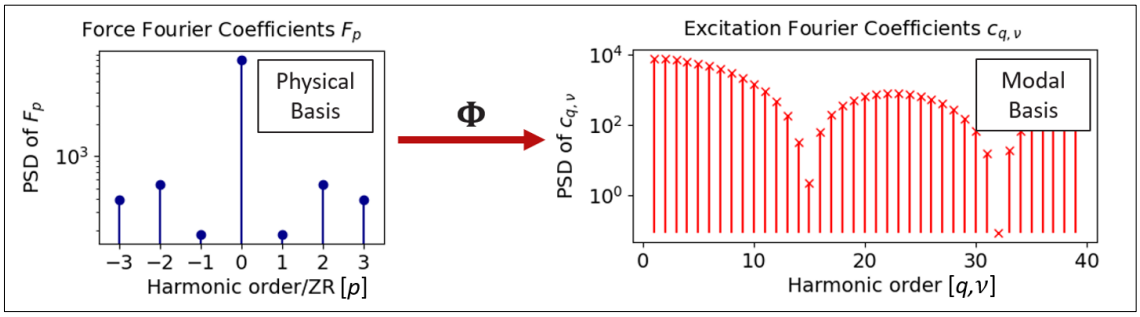

Figure 2: Transformation of the excitation from the physical to the modal basis

The resulting excitation harmonic magnitudes depend on their frequency proximity to corresponding natural frequencies $\omega_{\nu,\lambda}$,with mode $\lambda \in [1,\Lambda]$ of given normalized mode shapes $\boldsymbol{\psi}_{\nu,\lambda} \in \mathbb{C}^{N\times 1}$. The gyroscopic effect from rotation at frequency Ω causes each mode to split in conjugated backward ($\omega_{+\nu,\lambda}$ and $\boldsymbol{\psi}_{+\nu,\lambda}$) and forward ($\omega_{-\nu,\lambda}$ and $\boldsymbol{\psi}_{-\nu,\lambda}$) modes [4,14]. As developed in [4], the model deals with a single mode per nodal diameter. Here, the forced response model was adapted to a multimode λ contribution and expressed in the frequency domain in Eq. 2 and 3.

$$\boldsymbol{x}_{q,+\nu} = \sum_\lambda \frac{\sqrt{2\pi}}{\omega_{+\nu,\lambda}-(qZ_R+\nu)\Omega} \boldsymbol{A}_{+\nu,\lambda}\boldsymbol{c}_{q,+\nu}\delta[f-(qZ_R+\nu)\Omega] \tag{2}$$

$$\boldsymbol{x}_{q,-\nu} = \sum_\lambda \frac{\sqrt{2\pi}}{-\omega_{-\nu,\lambda}-(qZ_R-\nu)\Omega} \boldsymbol{A}_{-\nu,\lambda}\boldsymbol{c}^*_{q,-\nu}\delta[f-(qZ_R-\nu)\Omega] \tag{3}$$

In Eq. 2 and 3, $\boldsymbol{x}_{q,\nu} \in \mathbb{C}^{N\times 1}$ is the harmonic response, $\boldsymbol{A}_{+\nu,\lambda}$ and $\boldsymbol{A}_{-\nu,\lambda} \in \mathbb{C}^{N\times N}$ are the residual matrices of the λ^{th} forward and backward conjugated modes of nodal diameter ν, respectively. Residual matrices $\boldsymbol{A}_{\nu,\lambda}$ depend on normalized mode shapes $\boldsymbol{\psi}_{\nu,\lambda}$ as $\boldsymbol{A}_{\nu,\lambda} = \boldsymbol{\psi}_{\nu,\lambda}{\boldsymbol{\psi}_{\nu,\lambda}}^H$. For a given excitation periodicity, Eq. 1, 2 and 3 can be combined in a matrix form stacking all $N \times Q$ harmonics related to a given forward or backward nodal diameter ν as shown in Eq. 4:

$$\boldsymbol{X}_\nu = \sum_\lambda \boldsymbol{A}_{\nu,\lambda}\boldsymbol{F}\boldsymbol{\Phi}_\nu\boldsymbol{W}_{\nu,\lambda} \tag{4}$$

where $\boldsymbol{X}_\nu \in \mathbb{C}^{N\times Q}$ contains the response harmonics, $\boldsymbol{F} = [\boldsymbol{F}_0 \quad \boldsymbol{F}_{-p} \quad \boldsymbol{F}_p] \in \mathbb{C}^{N\times(2P+1)}$,, $p \in [1,P]$, contains the excitation Fourier coefficients, $\boldsymbol{\Phi}_\nu = [\boldsymbol{\phi}_0 \quad \boldsymbol{\phi}_{-p} \quad \boldsymbol{\phi}_p]^T \in \mathbb{C}^{(2P+1)\times Q}$ is the transformation matrix and $\boldsymbol{W}_{\nu,\lambda} \in \mathbb{R}^{Q\times Q}$ is a diagonal matrix with element $W_{qq} = \frac{\sqrt{2\pi}}{\omega_{+\nu,\lambda}-(qZ_R+\nu)\Omega}$ or $\frac{\sqrt{2\pi}}{-\omega_{-\nu,\lambda}-(qZ_R-\nu)\Omega}$ for backward or forward modes.

Francis turbines' excitation contains rotor-stator interactions (RSI), which are Z_G-periodic forces. To obtain an excitation model accounting for RSI, a Z_G periodicity is added to the 1Z model as: $\boldsymbol{X}_\nu^{1Z,Z_GZ} = \sum_\lambda \boldsymbol{A}_{\nu,\lambda}\boldsymbol{F}^{1Z,Z_GZ}\boldsymbol{\phi}_\nu^{1Z,Z_GZ}\boldsymbol{W}_{\nu,\lambda}$, where $\boldsymbol{X}_\nu^{1Z,Z_GZ} \in \mathbb{C}^{N\times Q}$ is the strain response matrix, $\boldsymbol{F}^{1Z,Z_GZ} = [\boldsymbol{F}^{1Z} \quad \boldsymbol{F}^{Z_GZ}] \in \mathbb{C}^{N\times 2(2P+1)}$ and $\boldsymbol{\phi}_\nu^{1Z,Z_GZ} = \left[\boldsymbol{\phi}_\nu^{1Z} \quad \boldsymbol{\phi}_\nu^{Z_GZ}\right]^T \in \mathbb{C}^{2(2P+1)\times Q}$ are respectively the combined 1Z and RSI force coefficients and modal transformation matrices. To infer the excitation coefficients $\boldsymbol{F}$,the error variance σ^2, the mode shapes $\boldsymbol{\psi}_{\nu,\lambda}$ and natural frequencies $\omega^\nu{}_\lambda$, the contribution of a specific excitation on the harmonics is isolated so that $\boldsymbol{X}_\nu = \boldsymbol{X}_\nu^{1Z,Z_GZ} - \mathbf{X}_\nu^{\bar{Z}}$.

3 Model-Based Inference Algorithm

The method used to fit the model to the measured strains synchronous harmonics of the runner is based on the Prediction Error Method (PEM) (see Eq. 5) [15]. The error $\boldsymbol{\varepsilon}$ between the measured harmonics $\widehat{\boldsymbol{X}}_\nu$ and the model $\boldsymbol{X}_\nu$ is proposed Gaussian $\boldsymbol{\varepsilon} \sim \mathcal{N}\left(0, \sigma^2\boldsymbol{I}_{2NQZ_R}\right)$.

$$\widehat{\boldsymbol{X}}_\nu = \boldsymbol{X}_\nu + \boldsymbol{\varepsilon} \tag{5}$$

Using Bayes' theorem [16] with a uniform prior, the posterior density of probability of the model given the data, $\mathcal{P}\left(\boldsymbol{X}_\nu, \sigma^2 \middle| \widehat{\boldsymbol{X}}_\nu\right)$, is expressed proportional to the likelihood $\mathscr{L}\left(\widehat{\boldsymbol{X}}_\nu \middle| \boldsymbol{X}_\nu, \sigma^2\right)$ of the data: $\mathcal{P}\left(\boldsymbol{X}_\nu, \sigma^2 \middle| \widehat{\boldsymbol{X}}_\nu\right) \propto \mathscr{L}\left(\widehat{\boldsymbol{X}}_\nu \middle| \boldsymbol{X}_\nu, \sigma^2\right)$. The resulting Complex Gaussian likelihood is expressed in Eq 6.

$$\mathscr{L}\left(\widehat{\boldsymbol{X}}_\nu \middle| \boldsymbol{X}_\nu, \sigma^2\right) \propto \frac{1}{\sigma^{2NQ}} e^{-\frac{1}{\sigma^2} tr\left[\left(\widehat{\boldsymbol{X}}_\nu - \boldsymbol{X}_\nu\right)^H \left(\widehat{\boldsymbol{X}}_\nu - \boldsymbol{X}_\nu\right)\right]} \tag{6}$$

From the likelihood, a conditional probability density is derived in sections 3.1 to 3.3 for the error, the excitation and mode shapes enabling Gibbs sampling [16]. Since the conditional probability density shape of the natural frequencies are unknown, as shown in section 3.4, a Metropolis-Hastings step is implemented leading to a Metropolis-Within-Gibbs algorithm [17].

3.1 Error Sampling Kernel

The error depends on all the harmonics of the response. Therefore, the conditional probability density is the product of every nodal diameter probability density. The obtained conditional probability density for the homoscedastic variance σ^2 is an inverse gamma distribution $\mathcal{G}^{-1}$ as shown in Eq. 7.

$$p(\sigma^2|\text{rest}) \propto \mathcal{G}^{-1}\left(\sum_\nu 2NQ - 1, \sum_\nu \left\|\widehat{\boldsymbol{X}}_\nu - \boldsymbol{X}_\nu\right\|^2\right) \tag{7}$$

3.2 Excitation Sampling Kernel

The excitation depends on every response harmonics. Eq. 8 expresses the conditional probability, $p(\boldsymbol{F}|rest)$, of the excitation using Eq. 6 and the model (Eq. 4) as $vec([Re(\boldsymbol{X}_\nu) \quad Im(\boldsymbol{X}_\nu)]^T) = \widetilde{\boldsymbol{P}}_\nu vec(\widetilde{\boldsymbol{F}})$:

$$p(\boldsymbol{F}|rest) \propto \mathcal{N}\left(\sum_\nu \left(\widetilde{\boldsymbol{P}}_\nu{}^T \widetilde{\boldsymbol{P}}_\nu\right)^{-1} \widetilde{\boldsymbol{P}}_\nu{}^T vec\left(\left[Re\left(\widehat{\boldsymbol{X}}_\nu\right) \quad Im\left(\widehat{\boldsymbol{X}}_\nu\right)\right]^T\right), \sigma^2 \sum_\nu \left(\widetilde{\boldsymbol{P}}_\nu{}^T \widetilde{\boldsymbol{P}}_\nu\right)^{-1}\right) \tag{8}$$

with $\widetilde{\boldsymbol{P}}_\nu = \left[Re\left(\sum_\lambda \boldsymbol{W}_{\nu\lambda}{}^T \boldsymbol{\Phi}_\nu{}^T \otimes \boldsymbol{A}_{\nu\lambda}\right) \quad Im\left(\sum_\lambda \boldsymbol{W}_{\nu\lambda}{}^T \boldsymbol{\Phi}_\nu{}^T \otimes \boldsymbol{A}_{\nu\lambda}\right)\right]^T \in \mathbb{R}^{2NQ \times 2N(2P+1)}$, the Kronecker product $\otimes$, and with $\widetilde{\boldsymbol{F}} = \left[Re([\boldsymbol{F}_0 \quad \boldsymbol{F}_p]) \quad Im\left(\boldsymbol{F}_p\right)\right] \in \mathbb{R}^{N \times (2P+1)}$.

3.3 Mode Shape Sampling Kernel

Mode shapes are complex vectors. Each mode λ has an associated mode shape. The conditional probability density for a given mode shape $\boldsymbol{\psi}_{\nu,\lambda}$ is evaluated with measured harmonics $\widehat{\boldsymbol{X}}_{\nu,\lambda}$ considering the contribution of other modes as described in Eq. 9.

$$\widehat{\boldsymbol{X}}_{\nu,\lambda} = \widehat{\boldsymbol{X}}_\nu - \sum_{\zeta \neq \lambda} \boldsymbol{A}_{\nu,\zeta} \boldsymbol{F} \boldsymbol{\Phi}_\nu \boldsymbol{W}_{\nu,\zeta} \tag{9}$$

From the proposed likelihood (Eq. 6), mode shape vectors contained in residual matrices $\boldsymbol{A}_{\nu,\lambda} = \boldsymbol{\psi}_{\nu,\lambda} \boldsymbol{\psi}_{\nu,\lambda}{}^H$ are factorized in Eq. 10 using the cyclic shift invariance of the trace.

$$\mathcal{L}\left(\widehat{\boldsymbol{X}}_{\nu,\lambda} \middle| \boldsymbol{X}_{\nu,\lambda}, \Sigma\right) \propto e^{tr\left[\boldsymbol{\psi}_{\nu,\lambda}{}^H \left(\frac{-1}{\sigma^2}\left[\boldsymbol{F}\boldsymbol{\Phi}_{\nu,\lambda}\boldsymbol{W}_{\nu,\lambda}\boldsymbol{W}_{\nu,\lambda}{}^T\boldsymbol{\Phi}_{\nu,\lambda}{}^H\boldsymbol{F}^H - \widehat{\boldsymbol{X}}_{\nu,\lambda}\boldsymbol{W}_{\nu,\lambda}{}^H\boldsymbol{\Phi}_{\nu,\lambda}{}^H\boldsymbol{F}_p{}^H - \boldsymbol{F}\boldsymbol{\Phi}_{\nu,\lambda}\boldsymbol{W}_{\nu,\lambda}\widehat{\boldsymbol{X}}_{\nu,\lambda}{}^H\right]\right)\boldsymbol{\psi}_{\nu,\lambda}\right]} \tag{10}$$

From Eq. 10, using Hoff (2009) developments, a vector Bingham conditional probability can be derived for a vector in $\mathbb{C}^{N\times 1}$, hence the normalized complex mode shape $\boldsymbol{\psi}_{\nu,\lambda}$.

3.4 Natural Frequency Sampling Kernel

The natural frequency $\omega_{\nu,\lambda}$ in the diagonal of $\boldsymbol{W}_{\nu,\lambda}$ has a intractable kernel shape as shown in Eq. 12.

$$\mathscr{L}\left(\widehat{\boldsymbol{X}}_{\nu,\lambda}\middle|\boldsymbol{X}_{\nu,\lambda},\Sigma\right) \propto e^{\frac{-1}{2\sigma^2}tr\left[-\boldsymbol{W}_{\nu,\lambda}\left(\widehat{\boldsymbol{X}}_{\nu,\lambda}{}^{H}\boldsymbol{A}_{\nu,\lambda}\boldsymbol{F}\boldsymbol{\Phi}_{\nu}+\boldsymbol{\Phi}_{\nu}{}^{H}\boldsymbol{F}^{H}\boldsymbol{A}_{\nu,\lambda}{}^{H}\widehat{\boldsymbol{X}}_{\nu,\lambda}\right)+\boldsymbol{W}_{\nu,\lambda}{}^{2}\boldsymbol{\Phi}_{\nu}{}^{H}\boldsymbol{F}^{H}\boldsymbol{A}_{\nu,\lambda}{}^{H}\boldsymbol{A}_{\nu,\lambda}\boldsymbol{F}\boldsymbol{\Phi}_{\nu}\right]} \tag{11}$$

Candidates ω_{ν,λ_i} at iteration i are sampled in a Gaussian distribution $\mathcal{N}\left(\omega_{\nu,\lambda_{i-1}},{\sigma_\lambda}^2\right)$, with a user defined variance ${\sigma_\lambda}^2$, in a random walk Metropolis-Hastings step [16]. To maximise the acceptance ratio of a given mode, variance ${\sigma_\lambda}^2$ can be defined mode specific considering the signal-to-noise ratio (SNR) of given harmonics. Forward modes have lower SNR because they are excited by higher order harmonics than backward modes. Therefore, inference of forward natural frequencies is more sensitive to stochastic excitation bias (see section 4.1.3). A hypothesis is made on mode-split, stating that the frequency gap between conjugate modes is in the range of 0 Hz to 10 Hz. A forward natural frequency density of probability $p\left(\omega_{-\nu,\lambda}|\text{rest}\right)$ is then weighted by a Gaussian prior $p\left(\omega_{-\nu,\lambda}|\omega_{+\nu,\lambda}\right) = -(\omega_{-\nu,\lambda}-\omega_{+\nu,\lambda})^2/2k^2$ given the backward natural frequency value $\omega_{-\nu,\lambda}$ and a user defined variance k^2 influencing $\omega_{\nu,\lambda}$ samples.

$$p\left(\omega_{-\nu,\lambda}|\text{rest}\right) \propto \mathscr{L}\left(\widehat{\boldsymbol{X}}_{\nu}\middle|\boldsymbol{X}_{\nu},\Sigma\right)p\left(\omega_{-\nu,\lambda}|\omega_{+\nu,\lambda}\right) \tag{12}$$

In the Metropolis-Hastings step of the algorithm, user-defined variances ${\sigma_\lambda}^2$ are tuned according to the noise level and the quantity of measurement points (sensors) considered for the inference to maximize the acceptance ratio of every natural frequency.

4 Synthetic Data Study

The probabilistic modal identification algorithm is intended to be deployed on *in situ* measurements. It, therefore, needs to be evaluated on a representative synthetic dataset. Three groups of parameters interreact for this instance, the excitation periodicities, the number of harmonics accessible from the measured response and the number of modes contained in the analyzed frequency band.

4.1 Range of Applicability

Probabilistic algorithm performance generally improves with larger datasets. The measured synchronous harmonics in the studied datasets are observed up to around the 40th to 50th harmonic. In this frequency range, for our studied Francis runner, 3 to 7 modes λ per nodal diameter ν are expected. In this sense, as the harmonic order considered by the algorithm increases, so does the complexity of the model to infer.

4.1.1 Minimal Quantity of Harmonics

Let's consider a system with two modes per nodal diameter, excited by a periodic force composed of a fundamental and three harmonics. This system is solved on five measured points on one blade. From the experimentation results, the minimal number of harmonics required for Markov Chain Monte-Carlo (MCMC) convergence is $Z_R Q$=39 for a Z_R=13 blades runner, e.g., Q=3 response harmonics per nodal diameter ν. When the periodic force is described by more harmonics in the spectral domain, the MCMC stability for the excitation decreases. This observation is also made when the number of observed measured points increases. However, this stability loss can be solved by adding higher-order response harmonics.

From the two mentioned limitations, the inference of a 2Z or RSI excitation from the $Z_R Q$~50 observable response harmonics in the response is unattainable. The one or two RSI-specific excitation harmonics observable can be ignored if still three harmonics per ND can be used for the inference. RSI excitation's amplitude contribution to 1Z-affected harmonics can be considered using a pseudo-inverse function to infer a residual amplitude for the RSI contribution to the harmonics.

4.1.2 Minimal Quantity of Modes

When the algorithm is tested on systems containing more than two modes per nodal diameter (ND), it causes a divergence in the excitation sampling. For a given nodal diameter ν , the modal residue induced by higher frequency modes introduces some inaccuracies in the inference, leading to a bias in the inference of the highest natural frequency, from now on called 2nd mode. The lowest natural frequency, e.g. first mode, is less altered suggesting that the higher frequency acts as a firewall that captures the higher frequency bias. A test was carried out where the algorithm tried to characterize two modes per ND from a synthetic signal containing the influence of four modes. Figure 3 illustrates the bias obtained for mode ND5-2. Without a frequency maximum constraint, some Markov Chains of the natural frequencies were also observed to drift towards higher frequencies in a multimodal shape.

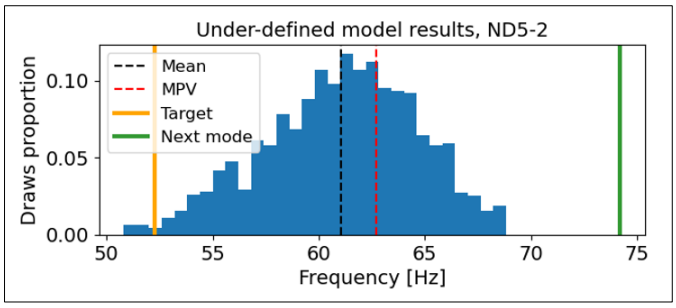

Figure 3: Algorithm mode under-definition bias effect on 2nd modes

To minimise the modal residue effect, forward and backward 2nd mode natural frequencies ND2-2 to ND6-2 are sampled using an independent Metropolis-Hastings method [16] based on a Gaussian distribution $\mathcal{N}\left(\omega_{\nu,2_{IW}}, {\sigma_\lambda}^2\right)$ with a constant defined mean $\omega_{\nu,2_{IW}}$ near the expected 2nd mode natural frequency and a variance ${\sigma_\lambda}^2$=100. A Gaussian prior $g\left(\omega_{\nu,\lambda}|\omega_{-\nu,\lambda}\right)$,given the conjugate mode, as initially defined for forward modes (section 3.4), is also added on all 2nd modes sampling. The additions constrain the 2nd modes sampling around the expected 2nd mode natural frequency value to minimize the modal under-definition and frequency variable stochasticity biases.

4.1.3 Stochastic Excitation Bias

On Francis turbine runner around the best efficiency point, stochastic excitations, dominated by periodic excitations, are marginal but non-zero. As the modelled excitation is proposed as purely periodic, the stochastic excitation contribution biases the model. The noise floor of strain measurements on an operating runner was analyzed at 70 %, 50 % and 20 % of guide vanes opening (GVO) to evaluate the stochastic excitation level at each opening. For the analysis, the measured stochastic contribution to the signal at the three guide vanes openings is normalized using the noise floor level $|2\gamma|^2$ near the first harmonic order in the power spectrum and the power of the first synchronous harmonic $|A_1|^2$ as $log[|2\gamma|^2/|A_1|^2]$. Noise floor levels in the range of 20 GVO to 70 GVO were observed between $log[|2\gamma|^2/|A_1|^2] =$ -7.5 and $log[|2\gamma|^2/|A_1|^2] =$ -9.2, hence a lower stochastic contribution near the BEP.

The algorithm's sensitivity to the stochastic bias was evaluated using added Gaussian stochasticity to the excitation for the tested GVO. The resulting absolute amplitude error for the excitation parameters is of order 10^{-2} to 10^{-1} for Gaussian stochastic contributions considered equivalent to 20 GVO and 70 GVO observations. As the amplitude of the periodic excitation's Fourier coefficient increases, the bias becomes negligible. The stochastic bias sensitivity analysis showed that the proposed Gaussian stochastic excitation has no critical effect on the excitation parameters around BEP, e.g. $log[2\gamma/|A_1|^2] \approx$-9, although the bias should be considered for better accuracy.

4.2 Synthetic Data Study Case

The algorithm is evaluated using the $3Z_R$ first harmonics produced by a four modes per ND, model under a combined 1Z and RSI excitation observed by 10 sensors. The forces are defined with fundamentals around $F_{0,1Z}$ =100 N·s, $F_{0,RSI}$=1000 N·s and five randomly generated harmonics. Turbine parameters are Z_G=24 guide vanes, Z_R=13 runner blades and a Ω=1.25 Hz rotating frequency. The observed RSI harmonic is considered using a pseudo-inverse function. To simulate a 70 % guide vanes opening, the stochastic excitation used generates a noise level of $log[|2\gamma|^2/|A_1|^2] =$ -8.13. Mode shapes are randomly generated, and natural frequencies are chosen in an actual runner-like range (see Table 1) based on previous modal analysis of the studied runner using finite element analysis in standstill water. In Figure 2, excitation harmonics generated by coefficients $\boldsymbol{c}_{q,v}$ are represented in red. Each harmonic's amplitude varies according to its proximity to the nodal diameter and companion-specific modes resulting in the strain response $\boldsymbol{X}_v$ in black. Forward modes harmonics are indicated by the minus sign. For visualization, the noise floor is represented among the harmonics. The probabilistic algorithm is set to infer the two firsts of the defined four modes per ND and three of the five defined excitation harmonics to reproduce an under-definition of the system as may occur on field measurements deployment.

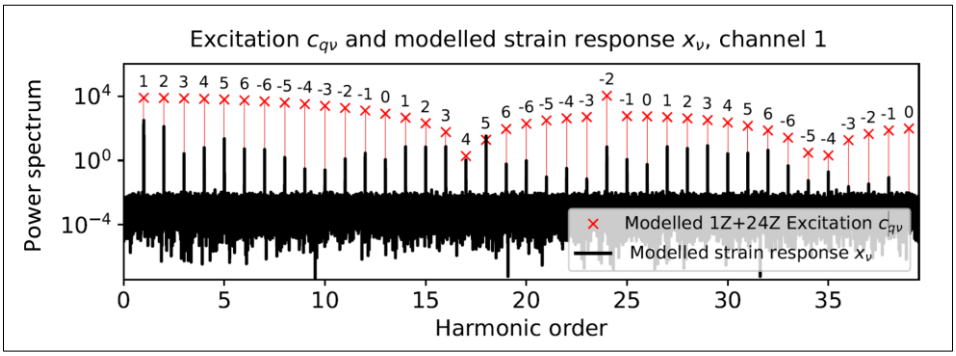

Figure 4: Excitation harmonics (red) modulated in the strain response (black)

4.3 Results on Synthetic Data

The model inference results are shown in Table 1. The Most Probable Value (MPV) per natural frequency is compared to the defined target value by a relative error in percentage.

Modes	Target [Hz]	MPV [Hz]	Error %	95% interval	Modes	Target [Hz]	MPV [Hz]	Error%	95% interval
ND1-1	8.0	7.2	10.4	6.9-11.0	ND1-2	27.0	28.9	6.9	20.3-29.5
ND1*-1	10.0	11.3	13.9	1.5-23.2	ND1*-2	31.0	31.8	2.5	16.3-41.0
ND2-1	12.1	13.3	9.8	10.8-14.8	ND2-2	48.0	45.4	4.5	41.0-53.3
ND2*-1	14.1	15.1	7.1	3.4-27.4	ND2*-2	53.8	48.9	9.1	37.0-59.0
ND3-1	22.0	22.1	0.5	22.2-23.7	ND3-2	50.2	49.1	2.2	45.3-62.1
ND3*-1	24.0	26.7	11.3	14.8-36.9	ND3*-2	53.8	55.1	2.4	45.5-67.1
ND4-1	27.2	25.8	5.3	22.3-28.5	ND4-2	51.9	44.8	13.6	48.8-64.8
ND4*-1	29.2	27.6	5.5	14.2-37.1	ND4*-2	55.2	53.6	5.8	45.5-67.1
ND5-1	29.4	30.5	3.7	28.8-33.6	ND5-2	52.3	61.0	20.0	52.2-65.8
ND5*-1	31.4	33.3	6.1	20.2-39.4	ND5*-2	56.9	60.4	5.5	48.5-67.8
ND6-1	30.2	31.7	5.0	26.8-36.8	ND6-2	52.1	55.6	6.7	51.0-63.3
ND6*-1	32.2	33.9	5.3	22.8-39.2	ND6*-2	57.3	57.0	1.6	48.0-67.6
ND0-1	9.5	19.7	108	3.9-38.5	ND0-2	30.0	53.6	78.6	29.8-69.3

Table 1 : Inferred natural frequencies from the modelled response

The Metropolis-Hasting candidate distribution for forward and backward modes ND2-2 to ND6-2 was set to a mean $\omega_{\nu,2_{IW}} = 50\ Hz$ and variance $\sigma_\lambda{}^2$=100 for the inference.

In Table 1, torsion modes (ND0) harmonics have poor Signal-to-Noise-Ratio (SNR) and lead to inconclusive results. Also linked to low SNR harmonics, forward modes ND1*-1 to ND6*-1 are inferred with a larger credibility interval, from 20 Hz to 25 Hz, than backward modes, from 2 Hz to 10 Hz. The resulting credibility intervals for 2nd modes, inferred with the independent candidate method, is in the range of 10 Hz to 25 Hz. The error over 13% of mode ND5-2 and ND4-2 results from the modal residue effect. Although the inferred 2nd modes may be biased, their consideration facilitates the inference of first modes as ND1-1 to ND6-1 are inferred within a 3 Hz error. The same analysis using 5 sensors showed similar results. Finally, the defined 2 % to 10 % mode split is within the error range.

5 Implementation on Field Measurements

The synthetic and the field measurements differ in the stochastic excitation influence and damping effects. To begin with, the stochastic excitation bias added to the model produces a constant broadband noise floor. In operation, turbulence excitation, cavitation and vortices might induce colored noise with an irregular floor. The biased harmonics might be interpreted of higher amplitude than expected by the model, increasing risks of excitation overshooting or indetermination. Furthermore, damping is not accounted for in the model. This omission might lead to phase biases of the inferred excitation and mode shapes, and to an overestimation of synchronous harmonics amplitude for a given natural frequency. The algorithm is deployed on field measurements to evaluate the impact of the biases.

5.1 Field Steady-State Strain Measurements

The studied runner is a low-head Francis turbine with Z_R=13 blades, Z_G=24 vanes and a rotating speed of Ω=1,25 Hz. The strain and pressure measures points are shown in Figure 4.

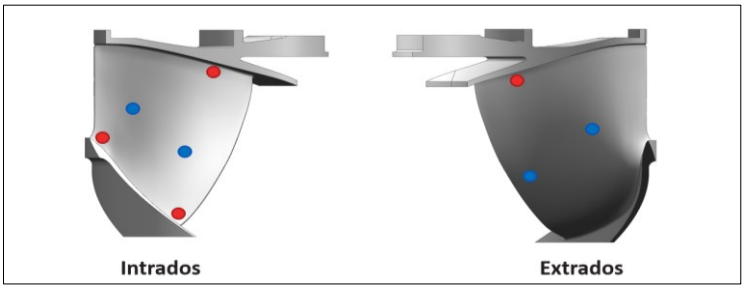

Figure 5: Strain (red) and pressure (blue) measured points

The pressure measurements are used to analyze the possible excitation periodicities in the runner. As shown in Figure 5-a, a dominant 1-per-revolution synchronous pressure amplitude is present in the system leading to the consideration that there is a 1Z excitation of the runner.

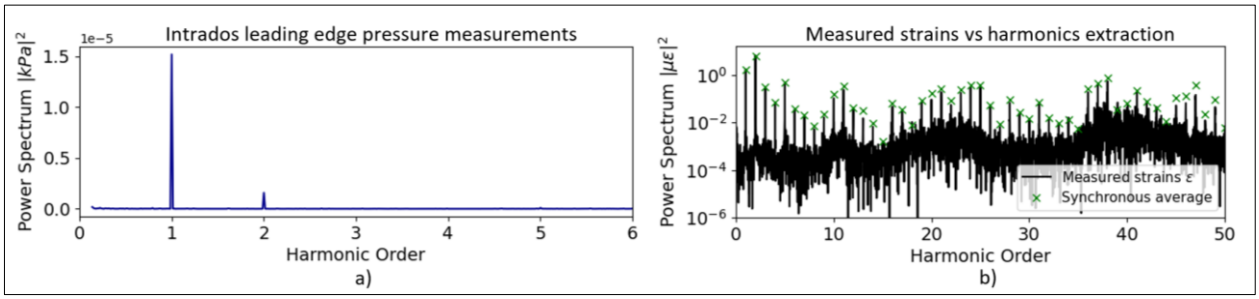

Figure 6: a) 30 cm from leading edge intrados pressure measurements on blade 2
b) Extracted harmonics (green) from measured strains (black)

The rotating speed of the runner is not perfectly constant. Some runners' rotating speed respond to the grid power variations or are oscillating around a speed command. The synchronous vibrations are then extracted by synchronous averaging. In Figure 5-b, in green are the extracted harmonic values from the response (black). The extracted harmonics are used for the inference of the model by the algorithm.

5.2 Results on Field Measurements

The excitation, mode shapes and natural frequencies inference is completed with measurements from five strain gauges on two blades of the same runner during stable operation near the best efficiency point. The algorithm is set to infer, over 200k iterations, 26 modes and a one-per-revolution (1Z) excitation, considering the RSI response harmonic, defined with one fundamental and three harmonics. The first 15 of the 26 inferred modes' natural frequencies of the runner are presented in Table 2. The inferred natural frequencies are compared to numerical simulation results of the studied runner in standstill water. As the numerical simulation did not include the runner shaft, simulated ND1 natural frequencies are not considered.

Modes	Sim. [Hz]	MPV Blade 1 [Hz]	Error %	95% interval	MPV Blade 2 [Hz]	Error %	95% interval	Blade difference [Hz]
ND1-1	-	5.5	-	4.5-6.4	4.1	-	4.0-12.2	1.4
ND1*-1		4.4	-	0.3-15.3	9.2	-	0.6-19.6	4.8
ND1-2	-	29.6	-	29.0-30.9	29.7	-	20.5-30.9	0.1
ND1*-2		31.7	-	19.2-41.6	25.4	-	16.9-67.4	6.3
ND2-1	12.0	8.7	27.6	7.8-12.6	8.5	29.2	7.2-8.8	0.2
ND2*-1		6.3	21.2	0.8-26.0	9.3	22.6	0.1-17.8	3.0
ND3-1	22.1	23.9	8.3	21.5-24.3	30.3	37.3	29.4-31.4	6.4
ND3*-1		17.4	6.9	8.3-30.1	21.9	0.8	9.8-34.2	4.5
ND4-1	27.2	31.4	15.3	22.9-34.5	29.3	7.6	24.2-39.5	2.1
ND4*-1		29.1	2.8	17.6-39.1	29.9	9.8	18.1-39.2	0.8
ND5-1	29.4	30.3	3.1	29.8-30.5	27.3	7.1	23.4-34.5	3.0
ND5*-1		28.6	2.7	18.2-38.4	29.4	0.0	17.1-38.8	0.8
ND6-1	30.2	26.8	11.3	25.6-27.8	29.5	2.4	27.1-37.0	2.7
ND6*-1		29.7	1.8	18.4-38.3	34.3	13.5	21.3-39.4	4.6

Table 2: Runner in steady-state operation inferred natural frequencies

From Table 2, the posterior distributions of forward modes natural frequencies ND2*-1 to ND6*-1 show a similar 20 Hz to 25 The MCMC of the excitation parameters showed partial stabilization. The reconstruction of the signal harmonics with the inferred model shows an up to 10^4 overshoot of the harmonics over the 13th order. These harmonics are mostly dependent on the second and third harmonics of the excitation.

On different tries with given measurements, a phase variability between the excitation Fourier coefficients and an up to 10 Hz variability of the inferred natural frequencies were observed. The blade difference presented in Table 2 may therefore not only be attributed to the local physical properties of the two blades but to the indetermination of the excitation with the actual model and data.

The varying noise floor and the omission of damping may be the root cause of the non-repeatability and the partial stabilization of the excitation entailing the need for the consideration of those effects. As the proposed model is shown non-exhaustive for the used measurements, the inferred modal parameters may not be statistically conclusive.

6 Discussion and Perspectives

The previous sections showed the inference of a periodic forced response model from synthetic data and operating runner strain measurements using a Bayesian inference-based algorithm. Although the inferred natural frequencies values are within the range of simulated natural frequencies, the method would benefit from future works to enhance the stability and resulting confidence intervals. Biases from stochastic excitations, modal residues and damping effects should be considered by the method. At first, stochastic excitations' contribution should be considered in the analysis as synchronous harmonics' amplitude might contain a non-negligible stochastic contribution that may cause the frequency-varying noise floor observed in the strain response (see fig 5-b). If the noise floor variations are mainly random, Discrete Random Separation (DRS) [19] could be used. Other noise floor models or the combination of the proposed deterministic harmonic modal analysis method and stochastic excitation-based traditional OMA could be of interest. This consideration could enhance the accuracy and range of applicability of the method in different operating regimes. Secondly, modal residue parameters should be added to the model as the algorithm is limited to the consideration of 2 modes. The consideration could lead to more accuracy in the 2nd modes inference. Thirdly, as damping may be difficult to include as a parameter in the probabilistic algorithm, sensitivity analysis or model selection methods using proposed damping constants added to the model could be of interest. As 2nd modes per ND may be more damped [8] the consideration of damping could correct the overshoot of the excitation and response harmonics by the algorithm.

The resulting more exhaustive algorithm could not only become a useful tool for operating runner's dynamics characterization but also represent a harmonic modal analysis opportunity on model scale runners. On model-scale test benches, it may be possible to generate a controlled 1Z excitation by moving a specific guide vane. With mechanical homology principles [20], the natural frequencies of operating runners could be deducted. This less expensive and more flexible application of the method could lead to new knowledge on runners' dynamics and loadings.

7 Conclusion

In operating hydro-turbines, Non-Trivial Runner-Casing Interactions (NTRCI) can produce a wide range of synchronous harmonics observable in strain gauge measurements of the runner's response. Dollon et al. (2023) proposed a periodic forced response model, considering gyroscopic effects, explaining the nodal diameter specificity and amplitude of the harmonics. In this paper, a Bayesian method is proposed to infer the roots of a periodic excitation, modal characteristics, and uncertainties of Dollon et al. (2023) NTRCI model from observed harmonics in a Francis runner steady-sate strain response. The proposed method is limited to a case study under a one-per-revolution (1Z -NTRCI) and Rotor-Stator Interaction (RSI) combined excitation with dominant influence from the 2 first modes of each specific nodal diameter. The proposed algorithm inferred 15 of the first modes of an operating Francis runner within a 5 Hz difference of simulated natural frequencies in standstill water and a 95% credible interval of 2 Hz to 25 Hz. The considered rotating frequency-dependent mode split effect was shown insignificant compared to the quantified uncertainties. The partial stabilization and non-repeatability of the excitation inference imply the non-negligibility of stochastic excitations, modal residue and damping effects.

Future works on stochastic excitation, modal residue and damping modelling could bring a more exhaustive physical model. The Bayesian inference algorithm could benefit from combined blade information in the statistical model and mode coupling information. Parameter discrimination could be enhanced by using model selection methods and prior information from numerical simulations as Bayesian algorithms are well suited for the addition of prior knowledge. Ultimately, this harmonic modal analysis method could bring more knowledge on runners' dynamics and loadings, essential for design, life analysis tools and health monitoring.

References

[1] Liu, X., Luo, Y., Karney, B. W., and Wang, W., 2015, "A Selected Literature Review of Efficiency Improvements in Hydraulic Turbines," Renewable and Sustainable Energy Reviews, **51**, pp. 18–28.

[2] Monette, C., Marmont, H., Chamberland-Lauzon, J., Skagerstrand, A., Coutu, A., and Carlevi, J., 2016, "Cost of Enlarged Operating Zone for an Existing Francis Runner," IOP Conference Series: Earth and Environmental Science, **49**, p. 072018.

[3] Savin, O., Baroth, J., Badina, C., Charbonnier, S., and Bérenguer, C., 2021, "Damage Due to Start-Stop Cycles of Turbine Runners under High-Cycle Fatigue," International Journal of Fatigue, **153**, p. 106458.

[4] Dollon, Q., Tahan, A., Antoni, J., Gagnon, M., and Monette, C., 2023, "Toward a Better Understanding of Synchronous Vibrations in Hydroelectric Turbines," Journal of Sound and Vibration, **544**, p. 117372.

[5] Châteauvert, T., Tessier, A., St-Amant, Y., Nicolle, J., and Houde, S., 2021, "Parametric Study and Preliminary Transposition of the Modal and Structural Responses of the Tr-FRANCIS Turbine at Speed-No-Load Operating Condition," Journal of Fluids and Structures, **106**, p. 103382.

[6] Gagnon, M., Dollon, Q., Nicolle, J., and Morissette, J.-F., 2021, "Operational Modal Analysis of Francis Turbine Runner Blades Using Transient Measurements," IOP Conf. Ser.: Earth Environ. Sci., **774**(1), p. 012082.

[7] Lais, S., Liang, Q., Henggeler, U., Weiss, T., Escaler, X., and Egusquiza, E., 2009, "Dynamic Analysis of Francis Runners - Experiment and Numerical Simulation," International Journal of Fluid Machinery and Systems, **2**(4), pp. 303–314.

[8] Valentín, D., Presas, A., Valero, C., Egusquiza, M., Jou, E., and Egusquiza, E., 2019, "Influence of the Hydrodynamic Damping on the Dynamic Response of Francis Turbine Runners," Journal of Fluids and Structures, **90**, pp. 71–89.

[9] Valentin, D., Presas, A., Bossio, M., Egusquiza Montagut, M., Egusquiza, E., and Valero, C., 2018, "Feasibility of Detecting Natural Frequencies of Hydraulic Turbines While in Operation, Using Strain Gauges," Sensors, **18**, p. 174.

[10] Graf, B., and Chen, L., "Correlation of Acoustic Fluid-Structural Interaction Method for Modal Analysis with Experimental Results of a Hydraulic Prototype Turbine Runner in Water."

[11] Brincker, R., and Ventura, C. E., 2015, "Introduction to Operational Modal Analysis: Brincker/Introduction to Operational Modal Analysis."

[12] Coutu, A., Roy, M. D., Monette, C., and Nennemann, B., 2008, "Experience with Rotor-Statorinteractions in High Head Francis Runner."

[13] Tanaka, H., 2011, "Vibration Behavior and Dynamic Stress of Runners of Very High Head Reversible Pump-Turbines," International Journal of Fluid Machinery and Systems, **4**(2), pp. 289–306.

[14] Louyot, M., Nennemann, B., Monette, C., and Gosselin, F., 2020, "Modal Analysis of a Spinning Disk in a Dense Fluid as a Model for High Head Hydraulic Turbines," Journal of Fluids and Structures, **94**, p. 102965.

[15] Ljung, L., 1987, "System Identification: Theory for the User."

[16] Bolstad, W. M., 2009, "Understanding Computational Bayesian Statistics: Bolstad/Understanding."

[17] Gilks, W. R., Best, N. G., and Tan, K. K. C., 1995, "Adaptive Rejection Metropolis Sampling Within Gibbs Sampling," Journal of the Royal Statistical Society Series C: Applied Statistics, **44**(4), pp. 455–472.

[18] Hoff, P. D., 2009, "Simulation of the Matrix Bingham–von Mises–Fisher Distribution, With Applications to Multivariate and Relational Data," Journal of Computational and Graphical Statistics, **18**(2), pp. 438–456.

[19] Antoni, J., and Randall, R. B., 2004, "Unsupervised Noise Cancellation for Vibration Signals: Part II—a Novel Frequency-Domain Algorithm," Mechanical Systems and Signal Processing, **18**(1), pp. 103–117.

[20] Valentín, D., Presas, A., Valero, C., Egusquiza, M., Egusquiza, E., Gomes, J., and Avellan, F., 2020, "Transposition of the Mechanical Behavior from Model to Prototype of Francis Turbines," Renewable Energy, **152**, pp. 1011–1023.